Modelling "Nano-Effects" in Sintering

Fan Li and Jingzhe Pan

Abstract Materials at the nanoscale typically show distinct behavior from their microsized counter parts. This is not different in sintering, and this chapter collects some previous studies on nano effects on this important phenomenon. It is constantly argued by researchers that classical continuum sintering model requires re-examination in the context of nanosintering. A possible way of doing this is by incorporating multiple mechanisms which may cause nano effects into the modeling. In this chapter we introduce both analytical and computational approaches. Analytical method is used to provide a guidance and first insight into nanosintering. Various computational models are then constructed using techniques such as Finite Difference (FD), Finite Element (FE), and Molecular Dynamics (MD), in order to capture the coupled features.

1 Introduction

The evaluation of the nanoscale effects on sintering can be done on an analytical basis by writing a more generic equation for its atomic movement. That is, solid state sintering is conventionally modeled using a diffusive flux, j, representing the number of atoms passing through a unit area per second (we are disregarding liquid phase sintering for now). Thanks to the understanding of sintering at the atomic level, this flux can be represented by an atomic driving force F, which equals to the spatial gradient of the chemical potential μ. The total flux of atoms in a general sintering process can then be related to the atomic concentration (C) and

F. Li · J. Pan (✉)
Department of Engineering, University of Leicester, LE1 7RH, Leicester, UK
e-mail: jp165@leicester.ac.uk

R. H. R. Castro and K. van Benthem (eds.), *Sintering*, Engineering Materials 35,
DOI: 10.1007/978-3-642-31009-6_2,

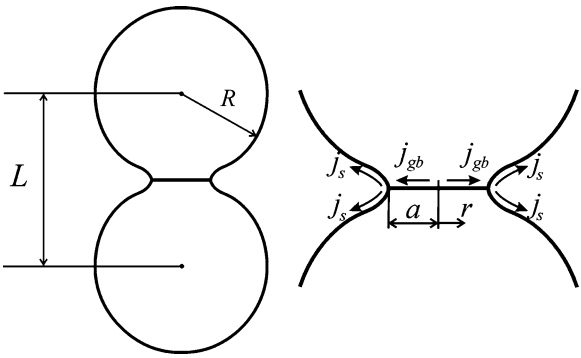

Fig. 1 Geometry of particle contact with two diffusion mechanisms

the atomic drift velocity (V) by $J = CV$. Since V is the product of the atomic jumping frequency (f) and the atomic spacing (a), we can write: $J = Caf$.

Since diffusion is driven by F, and the jumping frequency is dependent on the hyperbolic sine of F [1], we have:

$$j = \frac{2D}{a\Omega}\sinh\left(\frac{aF}{2kT}\right) = \frac{2D}{a\Omega}\sinh\left(-\frac{a}{2kT}\nabla\mu\right) \tag{1}$$

in which D is the diffusion coefficient depending on material constants and temperature, a and Ω are atomic spacing and volume, respectively, k is the Boltzmann constant, and T is the temperature in Kelvin.

The classical sintering theory assumes $aF \leq kT$, which leads to the linearization: $\sinh(aF/2kT) \approx (aF/2kT)$. A simplified linear diffusion law is therefore recovered:

$$j_{linear} = \frac{DF}{\Omega kT} = -\frac{D}{\Omega kT}\nabla\mu \tag{2}$$

Solving Eqs. (1) and (2) requires an explicit expression for the chemical potentials, μ. The gradient of μ along the diffusion route will be the driving force for mass movement. The chemical potential is a measure of the energy difference when one atom is added to a particular location. So, in absence of a concentration gradient, local excess energies will affect the chemical potential and lead diffusion.

Figure 1 shows two types of diffusions which are believed to play roles during the sintering process: grain boundary diffusion with flux j_{gb} and surface diffusion with flux j_s. The corresponding chemical potentials for these locations are [2]:

$$\mu = -\Omega\sigma \tag{3}$$

for the grain boundary (where σ is the stress normal to the grain boundary), and

$$\mu = -\Omega\gamma_s\kappa \tag{4}$$

for the free surface, where γ_s is the specific surface energy and κ the principal curvature of the free surface. As shown in Fig. 1, assuming a circular shape of

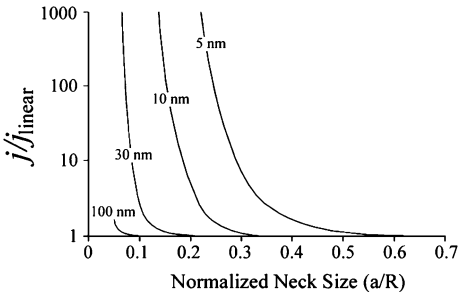

Fig. 2 Comparisons between linear diffusion law and non-linear diffusion law, for a typical set of sintering parameter of alumina. The sizes along the plots represent 'R'. Modified from Ref. [1]

grain boundary, the main curvature at the tip of the contact area can be described as [3]:

$$\kappa_{(r=a)} = 1/\rho - 1/a = 4R/a^2 - 1/a \tag{5}$$

in which r is the radial coordinate of the circular grain boundary, κ is the curvature of the particle profile, a the radius of grain boundary, and R the radius of the particle. The driving force at the edge of grain boundary can be estimated as:

$$F = \nabla\mu = \frac{\Delta\mu}{\Delta r} \approx -\frac{\mu_{(r=a)} - \mu_{(r=0)}}{a/2} = 2\gamma_s(4R - a)\frac{\Omega}{a^3} \tag{6}$$

A simple rearrange of Eq. (6) yields:

$$F = 2\gamma_s(4 - a/R)\frac{\Omega}{(a/R)^3}\frac{1}{R^2} \tag{7}$$

in which a/R is the normalized half neck size. Given a normalized neck size, the level of matter redistribution is determined for particles of any size. It can be then observed from Eq. (7) that the diffusion driving force F increases by the power of two with the decreasing of particle radius R. Therefore, there is potentially a huge driving force for the sintering of nanoparticles, i.e. particles with small values of R. If this is true, the approximation $aF \leq kT$ may not hold at these conditions and the linearization in Eq. (2) may have to be re-examined.

For the sintering of alumina with material parameters $a = 0.5$ nm, $\gamma_s = 1$ J/m^2, $\Omega = 0.02$ nm^3, at temperature T = 1160 K, Eqs. (1) and (2) can be solved separately through Eq. (6). The comparisons are shown in Fig. 2, where j obtained by the nonlinear law over that by the linear law is plotted against the normalized particle neck size. From the figure, it is evident that the linearization causes more error in calculating the driving force when both particle size R and neck size a/R are small. For particles of $R \geq 100$ nm however, the linearization is generally acceptable.

2 Densification Law

In the classical sintering theory, densification is believed to happen by the approaching motion of the particles, i.e., the change in the center to center distance, L, as shown in Fig. 1. Variational calculus is a convenient tool to solve this sort of problem [4–6].

Defining a total potential energy rate, Π, of a material under sintering as the summation of the power of the driving force over all migrating atoms and the changing rate of the total free energy E, we have:

$$\Pi = \sum_{all\_atoms} FV_{atom}(hdA/\Omega) + \dot{E} \tag{8}$$

in which V_{atom} is the atomic migration velocity, h is the thickness of the layer within which diffusion takes place, A is the area of the particle surface or grain boundary, and dot denotes the time derivative. Noticing that the diffusive flux $j = V_{atom}\, h\Omega$ and assuming linear diffusion law, Eq. (8) becomes:

$$\Pi = \int_S \frac{kT}{2\Omega D_s} j \cdot j dA + \int_{GB} \frac{kT}{2\Omega D_{GB}} j \cdot j dA + \dot{E} \tag{9}$$

in which D_{GB} and D_s are the diffusion coefficients at grain boundary and particle surface, respectively. The total free energy is reduced when two free surfaces turn into a grain boundary at a particle contact, i.e. we have $\dot{E} = -4\pi a\, \dot{a}\gamma_s$. $\delta\Pi = 0$ leads to [3]:

$$\left(\frac{\Delta L}{R}\right)^3 = 3\frac{\gamma_s D_{GB} h\Omega}{kTR^4} t \tag{10}$$

Equation (10) was first obtained by Coble [7] using the linear flux in equation (2) (Note that this is basically the same sort of derivation shown in the introductory chapter of this book for the lattice diffusion case). However, for the sintering of nanoparticles, the nonlinear flux in Eq. (1) may become important. Following Coble's [7] protocol, Eqs. (1) and (9) can be solved through numerical iterations. The results are plotted in Fig. 3. Interestingly, despite the huge error of flux using linear diffusion law for nanoparticles as shown in Fig. 2, the densification law is very similar, even for particle size as small as 5 nm. The figure shows densification as a function of time, hence the derivative (slope) represents the densification rate. The linear diffusion law yields the largest error at the beginning of the sintering and quickly catches up the nonlinear law, indicating a similar densification rate. It can be concluded that even for nanosized particles, the accuracy of classical linear diffusion law is acceptable, with a slight under-prediction of the sintering rate at the early stages.

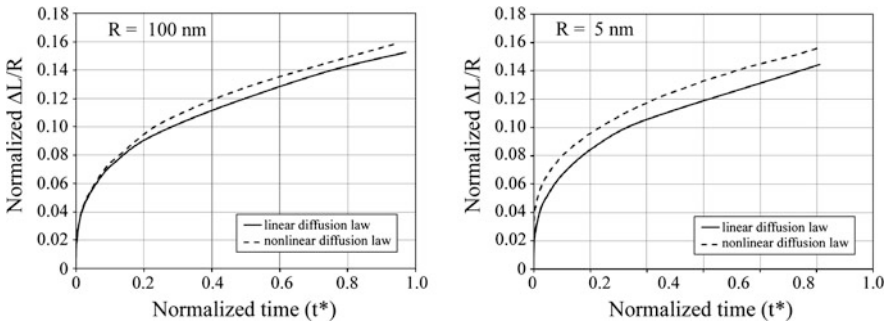

Fig. 3 Comparison between the linear solution (*solid lines*) and the nonlinear solutions (*dashed lines*) for the shrinkage between two spherical particles as functions of time, for different particle sizes

3 Nonlinear Relation Between Stress and Strain Rate

The densification equation can be further developed into a constitutive equation. For micron-sized particles, linear constitutive laws are often used to calculate sintering deformation. By considering a representative volume of a particle compact, the macroscopic stress–strain rate relationship in compact under sintering can be estimated from the total potential energy Π of the representative volume [8]:

$$\Pi = \dot{E}_{ij}\Sigma_{ij} - \frac{1}{v}\int_{GB}\frac{1}{2D_{GB}}j \cdot jdA - \frac{1}{v}\dot{E} \tag{11}$$

in which $\dot{E}_{ij}$ and Σ_{ij} are the macroscopic strain rate and stress, i and j are direction indices, and v is the volume of the macroscopic representative unit of the particle compact. Note that this equation does not include the surface diffusion term, as it can be generally assumed that surface diffusion is faster than grain boundary diffusion which controls the densification rate [9]. By relating the representative volume of the sintered body v to the relative density λ, Eq. (11) leads to a *viscous constitutive law* for solid state sintering [10, 11]:

$$\dot{E}_{ij} = \frac{36\Omega D_{GB}}{kTR^3}\Sigma_{ij}f(\lambda) + \dot{E}_{\exp} = \dot{E}_{0d}\frac{\Sigma_{ij}}{\Sigma_0}f(\lambda) + \dot{E}_{\exp} \tag{12}$$

where $\dot{E}_{\exp}$ is the free sintering strain rate, $\dot{E}_{0d}$ is a reference strain rate for the fully dense material under a reference stress Σ_0, $f(\lambda)$ is a non-dimensional function of the relative density λ, and the numeric parameter comes from assuming that the particles are of spherical shape.

For sintering processes under a large external force (such as in hot isostatic pressure assisted sintering, HIPing), the free sintering term in Eq. (12) can be ignored and a linear relationship between the strain rate and applied stress is predicted. Such constitutive law is therefore generally referred to be linear viscous

and widely used. On the other hand, it has been shown that in nanosintering with fine grains, the grain boundaries may not be the perfect sinks for vacancies (because they may have well defined structures) [12]. Hence atoms or vacancies can only be added to or removed from those sites as dislocations, resulting in climb of the dislocations in the boundary plane. In these cases, mechanisms at atomic level, such as viscous drag, or the action of friction and pinning forces may slow down the solid diffusion or even control the whole sintering process. Such mechanisms are referred to as "interface reaction" [12]. In the existence of interface reaction, the total chemical potential available to drive diffusion is reduced by an interface stress σ_r, and Eq. (3) becomes:

$$\mu = -\Omega(\sigma - \sigma_r) \tag{13}$$

By fitting existing experimental data, Cocks [13] suggested that the interface reaction stress follows a power law function of the separation rate $\Delta\dot{L}$ of particles:

$$\sigma_r = \frac{\sigma_0}{v_0^2}\Delta\dot{L}^2 \tag{14}$$

in which σ_0 is a reference stress, v_0 is the characteristic rate related to the interface reaction. If the diffusion is completely dominated by interface reaction, Cocks obtained the following constitutive law [12]:

$$\dot{E}_{ij} = 0.772\frac{v_0}{R}\left(\frac{\Sigma_{ij}}{\Sigma_0}\right)^2 g(\lambda) + \dot{E}_{\exp} = \dot{E}_{0i}\left(\frac{\Sigma_{ij}}{\Sigma_0}\right)^2 g(\lambda) + \dot{E}_{\exp} \tag{15}$$

in which g(λ) is a non-dimensional function different from $f(\lambda)$, $\dot{E}_{0i}$ is a reference strain rate for the interface reaction controlled process. As indicated by Eq. (15), if $\dot{E}_{\exp}$ is ignored, the stress–strain rate relationship follows a power law of exponent 2, rather than being linear in the diffusion controlled densification [Eq. (12)]. The ratio between the reference strain rates of the two mechanisms is given by:

$$\frac{\dot{E}_{0d}}{\dot{E}_{0i}} = \frac{46.5 D_{GB} V_M}{kTR^2 v_0}\Sigma_0 \tag{16}$$

which can be used as an indicator for the relative importance of the two mechanisms. When $\dot{E}_{0d}/\dot{E}_{0i}$ is large, the interface reaction consumes more energy than the diffusion process. The interface reaction therefore controls the sintering rate. Judging from Eq. (16), for small grain-size and lower temperature, the sintering process is more likely to be dominated by interface reaction. The experimental data in Ref. [14] (see Fig. 3 in Ref. [14]) shows that the power exponent in the stress-strain rate relation changes from 1 to 2, indicating a switch of mechanism in the half way of sintering. For nano-powder compacts, the stress–strain rate relationship may become nonlinear due to the dominance of interface reaction.

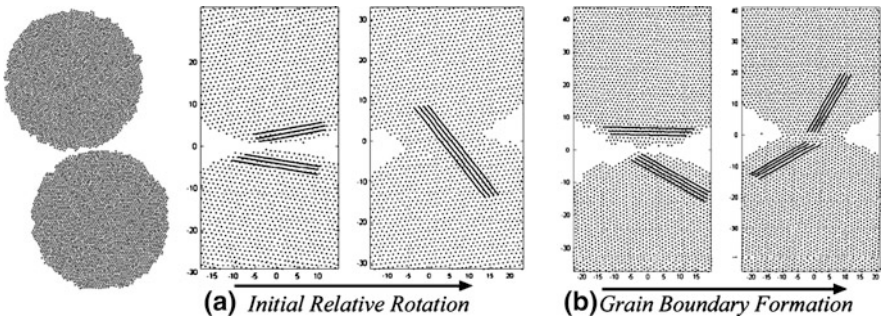

Fig. 4 Two kinds of contact formed between nanoparticles in sintering **a** a low energy perfect atomic alignment and **b** a high energy 'miss oriented' grain boundary

4 A Molecular Dynamics Study of Sintering

The diffusion law expressed by Eq. (1) and the densification law expressed by Eq. (11) are based on the assumption that grain boundary diffusion and surface diffusion are the two mechanisms controlling the whole diffusion process. This continuum treatment of the atomic migration can be naturally assessed by molecular dynamics (MD) studies [15]. The MD model of particles in sintering is illustrated in Fig. 4. The particle diameter is about 16 nm. An interesting observation from these MD simulations is that the contact area between the two particles can reach a low energy state in the very beginning of the sintering process and form a perfectly aligned interface. As shown in Fig. 4a, for particles with different initial crystalline orientations, a quick adjustment in the atomic orientations can occur at the very beginning of the sintering. The particles then remain in the adjusted orientations throughout the rest of the sintering process (Fig. 5a). This reorientation has been also observed in nanosintering experiments [16]. In some other cases, a non-coherent grain boundary is formed after the initial adjustment, as shown in Fig. 4b. It is observed that three factors can help the formation of a grain boundary: (i) large initial misalignment angle between particles, (ii) relatively large particle size, and (iii) high sintering temperatures.

Snapshots of the simulated sintering process are presented in Fig. 5. The following colouring scheme is used: the bulk atoms are always coloured as blue, any atom that has been on either the particle surface or the particle interface is colored as red, and any atom that has ever been into the vapor is colored as cyan. The coloring scheme therefore provides a rough picture of the matter redistribution during the sintering process. For Fig. 5a, since the crystalline structures of both particles are aligned at the very beginning of the sintering process, there exists no fast diffusion route between the two particles, as detailed in Fig. 4a. The sintering process started with a quick neck formation followed by neck growth firstly by surface diffusion and then by vapor condensation. However these matter redistribution mechanisms do not make the two particles to approach each other. For the second case there is a grain boundary acting as the fast diffusion route between two

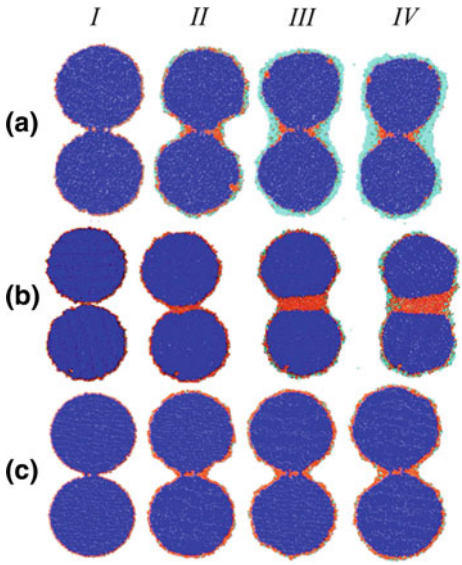

Fig. 5 MD simulation of two nanoparticles in sintering **a** high temperature without grain boundary, **b** high temperature with grain boundary and **c** low temperature (73 % to that of (**a**) and (**b**)) without grain boundary. (I–IV) shows different sintering times (same times for all the three cases); see text for the coloring scheme. Adapted from Ref. [15]

the contacting particles (Fig. 5b), the neck is filled up dominantly by atoms coming from the particle interface. Grain boundary diffusion is the controlling mechanism and the two particles approach each other. A case of lower sintering temperature is shown in Fig. 5c, where it is difficult to form a grain boundary between the two particles and vapor evaporation is also much weaker. Surface diffusion is the dominant mechanism of material redistribution. Further measurements confirm that if the atomic orientations of the two particles are perfectly aligned, such as that shown in Figs. 5a, c, the distance between the two particles remains unchanged during the sintering process. This is consistent with the established continuum theory that densification is only observed by grain boundary diffusion [9]. However, what the continuum theory cannot predict is the crystalline orientation of the particles and therefore unable to predict the sintering behavior of the nano-particles. These three cases shown in Fig. 5 therefore highlight the difference between the MD models and the continuum models for sintering of nanoparticles.

For nanoparticles, the sintering behavior observed in the MD simulations is therefore beyond the predictability of the continuum theory. If the assumed mechanism of matter redistribution in a continuum model does occur in a MD simulation, then it would be interesting to see if the two models agree with each other. Figure 6 compares the neck growth as a function of time predicted by continuum and MD models respectively. Figure 6a shows a case where matter redistribution is controlled by grain boundary diffusion, corresponding to Fig. 5b. Figure 6b shows a case controlled by surface diffusion corresponding to Fig. 5c. The straight lines are the continuum models while the discrete dots were obtained from several independent MD simulations. It is remarkable to see that the continuum models work reasonably well for nanoparticles, though it is clear that there is a change in the slopes of MD calculation that cannot be fitted by the continuum models.

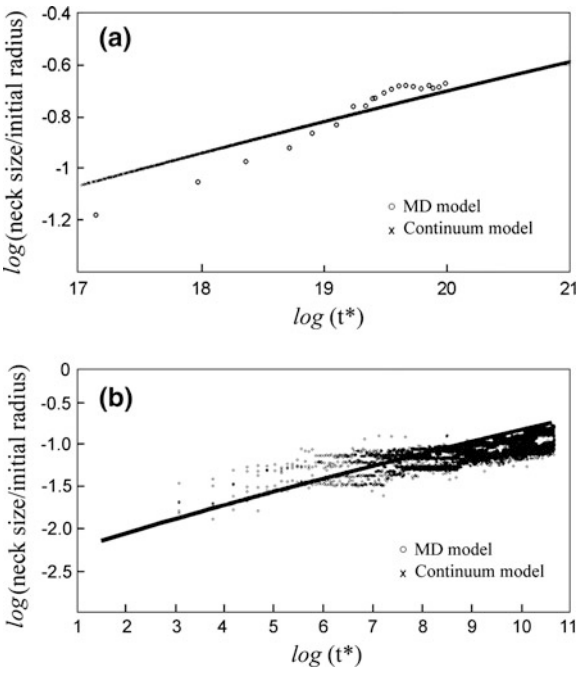

Fig. 6 Normalized neck size as a function of normalized time calculated by the MD model (*discrete dots*) and continuum model (*solid line*) for the sintering of two particles **a** high temperature sintering controlled by grain boundary diffusion and **b** low temperature sintering controlled by surface diffusion. Adapted from Ref. [15]

5 Coarsening Law

Particle/grain coarsening is another important phenomenon in nanosintering. It is important to maintain the nano-size of the particles to obtain a nanostructure for the sintered material. Practically the sizes of the particles are not as uniform as illustrated in Figs. 1 and 4. When a large particle meets a smaller one, classical sintering theory predicts that the grain boundary migrates towards the small particle and the size of large particle increases [17–19]. Nano-effect may also play a key role in the particle coarsening process.

According to Ref. [20], energy dissipation by grain-boundary migration can be reflected by an additional term in the variational functional in Eq. (9):

$$\Pi = \int_S \frac{1}{2D_s} j \cdot j dA + \int_{GB} \frac{1}{2D_{GB}} j \cdot j dA + \int_{GB} \frac{h}{2\tilde{M}} v_\perp \cdot v_\perp dA + \dot{E} \tag{17}$$

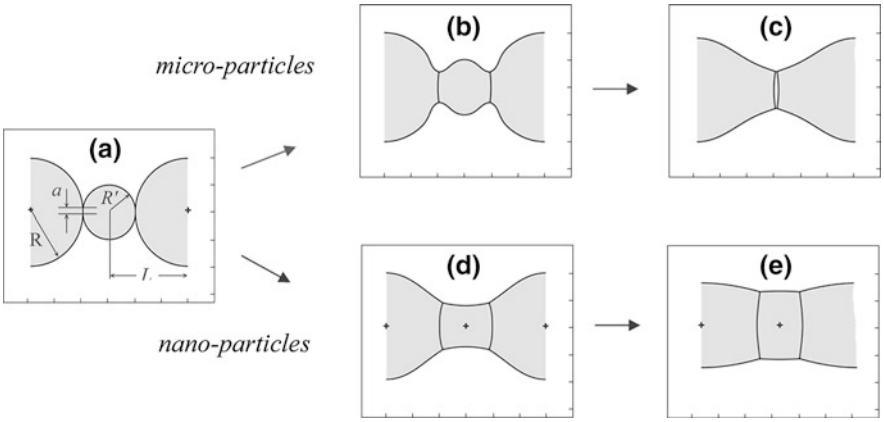

Fig. 7 Computer simulated shape evolutions of nano-sized particles of different sizes. **a** initial configuration, **b**, **c** micron size particles at different sintering stages, **d**, **e**, nano size particles at different sintering stages. Adapted from Ref. [20]

in which $v_\perp$ is the atomic migration velocity normal to the particle interface which leads to grain boundary migration and $\tilde{M}$ is the grain boundary mobility. A non-dimensionalisation analysis leads to [20]

$$\Pi^* = \int_S \frac{1}{2D_s^*} j \cdot j dA + \int_{GB} j \cdot j dA + \int_{GB} \frac{1}{2\tilde{M}^*} v_\perp \cdot v_\perp dA + \dot{E}^* \tag{18}$$

in which

$$D_s^* = D_s/D_{GB}^*, \ \tilde{M}^* = \tilde{M}R^2/hD_{GB} = (R/h)^2, \ E^* = E/D_{GB} \tag{19}$$

In Eq. (18), $\tilde{M}^*$ serves as an indicator for a size effect during particle coarsening. For grain boundary migration, atoms only have to move slightly normal to the grain boundary in the range of the grain-boundary thickness h, which is in the order of a few nanometers. For the grain boundary diffusion, on the other hand, atoms have to move along the grain boundary in a tangential direction, which has the length scale of the particle size, $a^2 \approx \Delta L/R$ (see Fig. 1). Reducing the particle size therefore has a huge effect on grain boundary diffusion but almost no effect on grain-boundary migration. Reference [20] derived a numerical scheme to solve Eq. (18). Their results are shown in Fig. 7.

Coarsening was simulated using a model of a small particle located in the middle of two large neighboring particles. The radius of the large particles is twice the small one. Two different particle sizes are used in Fig. 7 to illustrate the size effect. For the large particles with sizes equal 1 μm, it can be seen from Fig. 7b, c that the grain boundary continually moves towards the small particle. The large particles invade into the small one and finally only a small fraction of the small

particle remains. This is consistent with classical particle coarsening theory during sintering. For the nanoparticles shown in Fig. 7d, e, however, the coarsening behavior is more complicated. The small nanoparticle shows certain resistance to invasion. The curvature of the surface of the small particle changes direction from Fig. 7d, e, indicating that the small particle was taking materials from the surfaces of the large particles through surface diffusion up to certain stage. This occurs only in the nanoparticles because of the short diffusion distance (the actual size of the particles in Fig. 7d, e is three order of magnitude smaller than that in the Figures above them). The small particle then grows, rather than shrinks, at the expense of the two large particles. At the final stage, the small particle eventually decreases in size, leading to the coarsening of two large particles.

This interesting phenomenon of resistance to coarsening by nanoparticles can be seen more clearly in Fig. 8, which compares the coarsening behaviors for particles of different sizes of two different particle arrangements. A log plot is used in order to include all particle sizes in one figure. The points *b*, and *c* in Fig. 8 correspond to Fig. 7b, c. For the particle arrangement shown in Fig. 7a, the small particle can increase its size rather than decreasing it. It can be seen from Fig. 8 that the smaller the particle size is, the larger resistance it has to coarsening. However, if a different particle arrangement is assumed, such as one large particle in contact with one small particle, there is no resistance to coarsening at all as shown by the broken lines in Fig. 8. A parallel study of densification law [20] (which is not shown here) in the existence of coarsening also suggests that densification law may be very different when assuming different particle contact, such as in Fig. 8. These numerical studies suggest that densification law and coarsening law cannot be considered separately, which has been a standard practice in the existing sintering theory.

6 Pre-Sintering Agglomeration

The numerical simulation above shows that the nanoparticle exerts certain degree of resistance to coarsening. This has also been reported in experiments [21]. However at the same time, it has been also reported that there is severe coarsening of nanoparticles [22]. Such contradiction can be attributed to the agglomeration state in the pre-sintering powder. As the size of particles gets smaller, the surface interaction between fine particles makes them very 'sticky' and difficult to separate.

As shown in Fig. 9, the agglomeration can be modelled using two particle contact, which is very similar to the diffusion model in Fig. 1. Size effect is studied by assigning a kinetic energy to the particles about to contact each other. Whenever the particles meet each other, that kinetic energy is converted into neck formation. A neck is formed by either elastic or plastic deformation and total free energy associated with the surface energy is reduced. Continuum theory predicted that the force required to separate adhered particles is in between $-2\pi R\ \gamma_s$ and

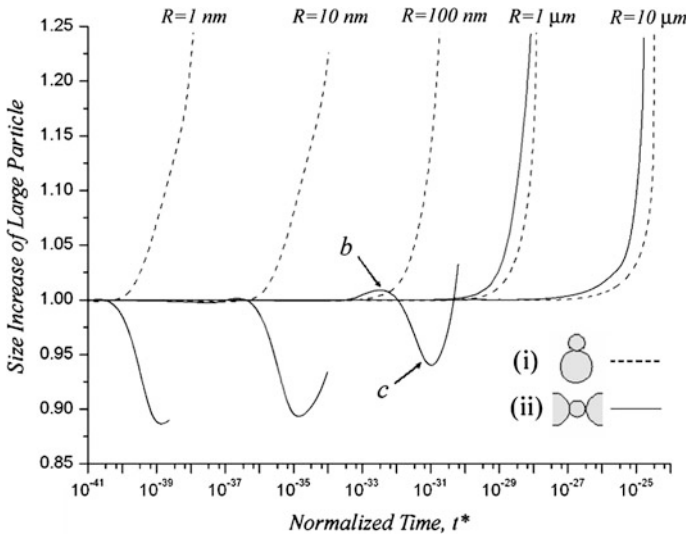

Fig. 8 Particle size (normalized by its original size) versus normalized sintering time. The solid lines were obtained using a model of one small particle placed between two large ones and the *dashed lines* were obtained using a model of one large particle in contact with a small one model. **b** and **c** correspond to the stages of the particle evolution shown in Fig. 7b, c. Adapted from Ref. [20]

$-1.5\pi R\ \gamma_s$ [23–26], recalling that γ_s represents the specific surface energy. If we ignore the effect of the surface energy, the particles will always rebound after impact. However a smaller particle has a higher proportion of surface energy comparing to the elastic strain energy. The surface energy effect becomes more important for small particles and is responsible for the sticking and agglomeration between small particles.

The coupled problem of particle interaction under the combined effects of surface energy and elastic deformation energy can be solved numerically using the Finite Element method [27, 28]. The force–displacement curve is plotted in Fig. 9a–c for different particle sizes using a common value for the specific surface energy of $\gamma_s = 0.11$ J/m^2. The results are normalized by the particle size. The surface energy and deformation energy can be measured as the area under the contact force–displacement curves. It can be seen from Fig. 9 that the work done by surface energy is more important for smaller particles, explaining the higher agglomeration of the nanoparticles.

The Maugis contact law that takes into account of particle adhesion is also plotted in Fig. 9 [28]. It appears that the analytical model works fairly well for nanoparticles. However, particle surfaces are never atomically smooth. It is therefore important to understand the effect of surface roughness on the particle adhesion. As shown in Fig. 10, the contact between rough surfaces can be modeled as contact between the asperities of the surfaces. The effect of roughness is here considered using two identical particles of 50 nm in the enveloping radius with

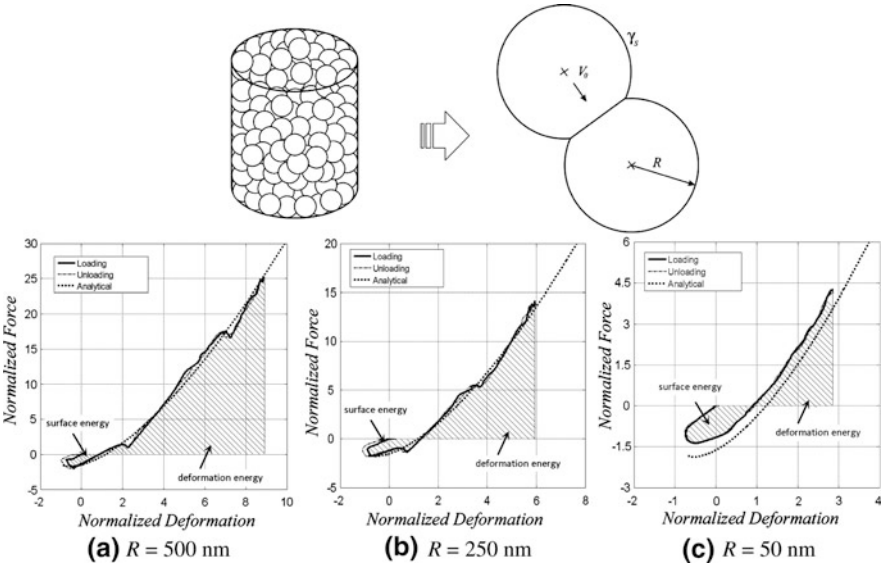

Fig. 9 Contact force versus particle deformation for adhesive contact between particles of different sizes: **a** R = 500 nm, **b** R = 250 nm and **c** R = 50 nm. Shaded areas represent kinetic energy (positive) and surface energy (negative)

sinusoidal asperities of about 1 nm in height of two different periods [28]. The specific surface energy is taken as $\gamma_s = 1.17$ J/m^{2,} which is roughly the nominal value for metallic particles such as copper. The shape of the force–displacement curve in Fig. 10a is very similar to the one in Fig. 10c. The whole kinetic energy is fully recovered at the end of contact, represented by a zero deformation at the end of unloading curve. For the Fig. 10b, on the other hand, the final unloading deformation is not zero, indicating particle adhesion. This is a typical adhesive behaviour in which the kinetic energy is not large enough to overcome the surface energy. The two cases are designed to demonstrate that a slight difference in surface roughness can change the behaviour of the particles from non-sticking (Fig. 10a) to sticking (Fig. 10b). The particles with more asperities (Fig. 10a), i.e. a rougher surface, behave like particles with smaller specific surface energy as those shown in Fig. 9c. Using an effective value of specific surface energy it is possible to fit the numerical results with the Maugis contact law. This is shown in Fig. 10a, b by taking $\gamma_{eff} = 0.19$ J/m^2 and $\gamma_{eff} = 0.26$ J/m^2 respectively. The analytical solution would work well if a relation between the surface roughness and the effective specific surface energy can be established.

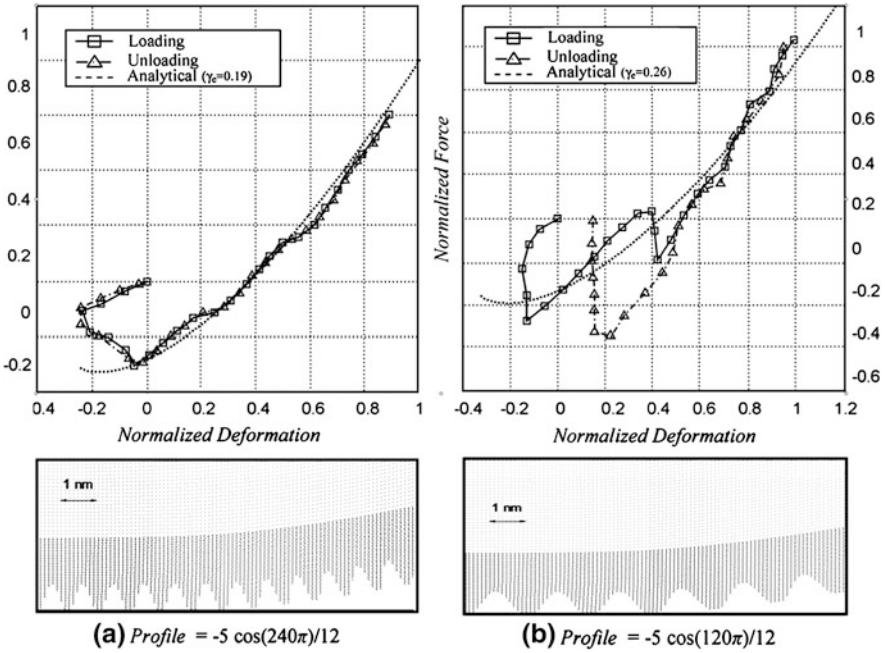

Fig. 10 Force plotted again deformation for particles ($R = 50$ nm) with a rough surface near the contact area with different degrees of roughness. **a** a rougher surface, and **b** less rough surface. Analytical solution using an effective surface energy is also plotted for comparisons

7 Closing of Large Pores

A consequence of agglomeration is that it is difficult to achieve dense packing for a pre-sintering nanoparticle system. During the sintering process, a common problem is that large pores are left behind the sintering of which requires long time and destroys the nanostructure by grain-coarsening. Sintering kinetics of the large pores could be a key concern for controlling the densification behaviour of all granulated powders [29]. A text book theory of sintering of large pores can be explained using the configuration in Fig. 11 of the previous chapter. If we refer to the number of grains surrounding a pore, i.e. the coordination number, as n, a pore is said to be large if n is large. For a small change in pore radius referred to as Δr, the total free energy change will be the difference between the increase in the interface energy associated with the grain boundaries and the decrease of the total surface energy:

$$\delta E = n\delta r\gamma_{gb} - 2\pi\delta r\gamma_s \tag{20}$$

Pore shrinkage requires the reduction of total energy $\Delta E < 0$, which leads to

$$n < 2\pi\gamma_s/\gamma_{gb} \tag{21}$$

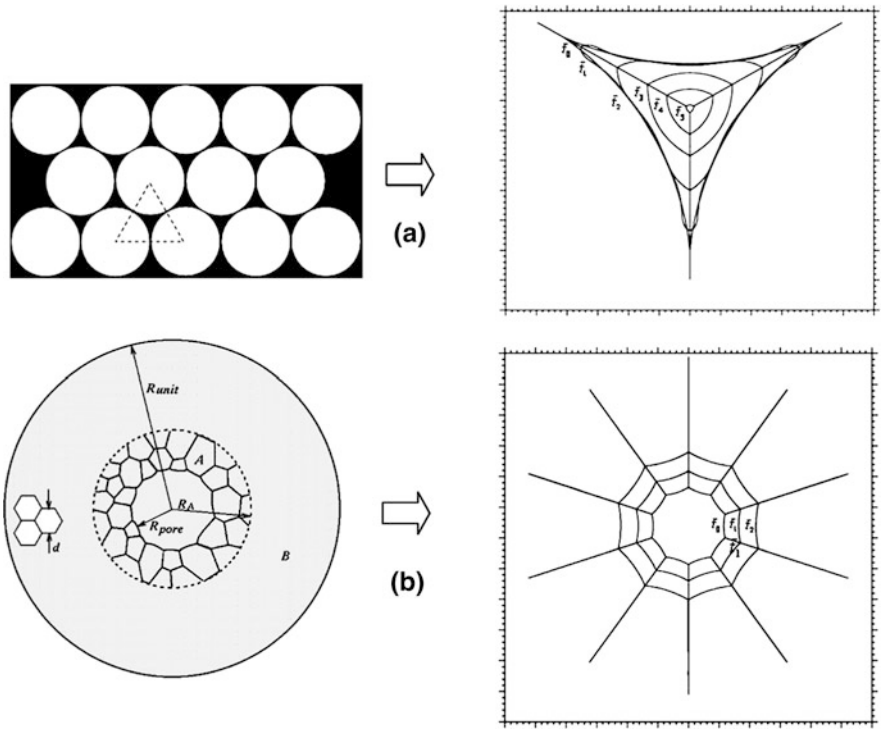

Fig. 11 Computer simulated evolutions of pores surrounded by symmetrical grains with two different coordination numbers. $\bar{t}_i$(i = 0, 1, …) indicates time sequence. **a** Pore with a coordination number of three shrinks and **b** pore with a coordination number of ten grows

A parallel argument is that only if the surface of the grains surrounding the large pore is "concave" does the pore shrink. It is therefore predicted that there exists a critical coordination number, which depends on the dihedral angle of the material. A pore will shrink only if its coordination number is less than the critical value Eq. (21). For a powder compact, the critical coordinate number is predicted according to the dihedral angle, which is a material constant. It follows that a large pore can only be eliminated after sufficient grain-growth, which reduces the coordination number to be under the critical value. There are two simplifications in the critical coordination number theory: (i) the large pore is surrounded by identical grains, and (ii) the grains move simultaneously during size changing of a large pore. It turns out that these simplifications are one step too far in understanding the behavior of any real powder compact.

In the past decades, increasing experimental evidence contradicts the critical coordination theory [30–32]. Pan and coworkers used their numerical methods described previously and studied what occurs if these simplifications are dropped [33, 34]. As shown in Fig. 11, two different initial configurations of pores with different coordination numbers are constructed. Grain boundary diffusion, surface

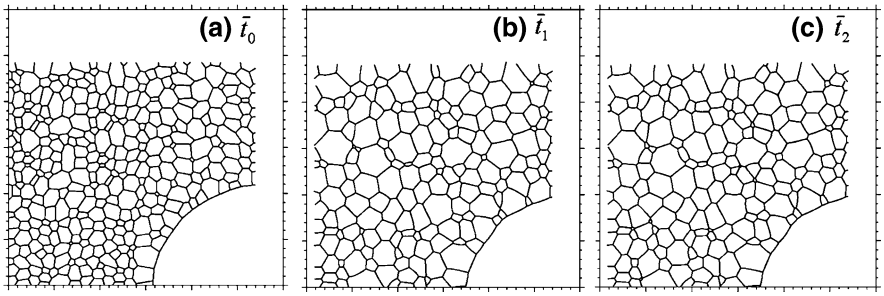

Fig. 12 Computer simulated evolutions of pore surrounded by a random arrayed grains: **a** initial configuration at time $\bar{t}_0$, **b** configuration at time $\bar{t}_1$, and **c** configuration at time $\bar{t}_2$. Taken from Ref. [34]

diffusion, and grain boundary migration are considered by solving Eq. (18). It is clearly shown in Fig. 11 that if the grains surrounding the pore are symmetrically arranged, the critical coordination number works well: the pore with small coordination number shrinks while the pore with large coordination number grows.

For a real powder compact, it is unrealistic to model the pore-grain matrix as shown in Fig. 11, i.e., there is no such symmetrical condition. For a network of random grains with roughly equiaxed shape, the strong symmetrical assumption is relaxed in Fig. 12. With time sequence from Fig. 12a–c, it is clear that the large pore shrinks despite its very large coordination number. A continuum version of the large pore model is shown in Fig. 13. The sintering stress σ_s exists due to the tendency for the large pore to reduce its surface and hence associated free energy. Material containing a large pore can be modeled by a hollow sphere [34]. The initial grain-size in Fig. 13b is 250 nm and the pore size varies from 20 to 125 μm. Figure 13c compares the analytical solution with the experimental data [32].

These studies conclude that large pores always shrink because there is always a thermodynamic driving force to eliminate the pores regardless of its coordination number. This does not mean that one can expect to eliminate the large pores through extended sintering. The time required for eliminating these large pores can be unrealistically long during which other events, such as coarsening, can take over. It does mean, however, that promoting grain-growth during sintering is always counter-productive if one wants to achieve densification.

8 Concluding Remarks

Modelling sintering of nanopowders is a challenging task where many text book theories need to be re-examined. The studies presented in this chapter are certainly far from a complete understanding. In terms of the validity of existing sintering theory for nano-particles, a somewhat obvious conclusion emerged from these previous studies, that is, the behavior of nanoparticles during the sintering process

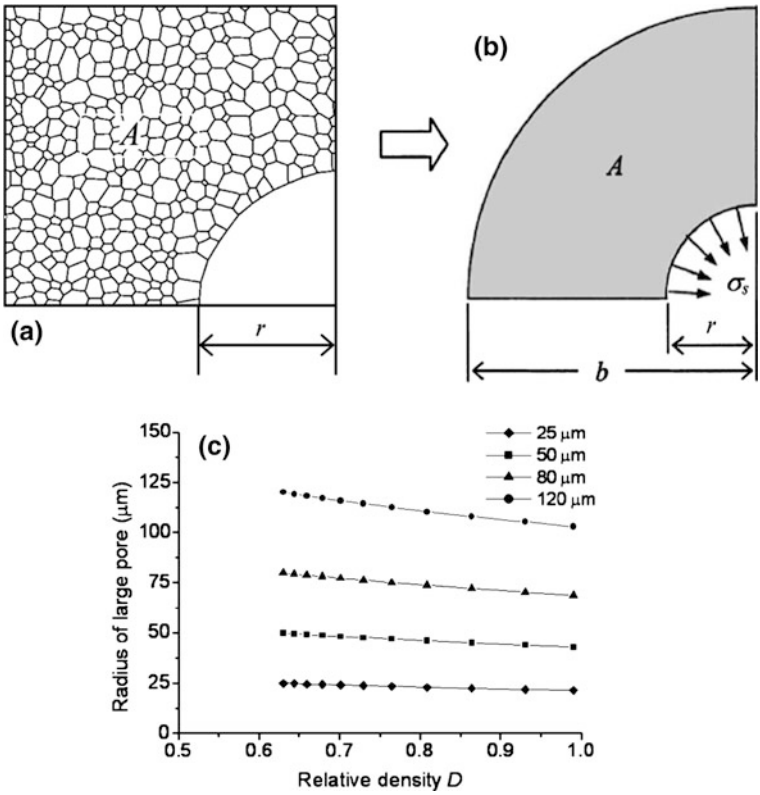

Fig. 13 An analytical model for the sintering of large pore: **a** discrete model, **b** continuum hollow sphere model, and **c** comparison with experiments showing the shrinkage of large pores for different pore sizes (with initial grain-size 250 nm), From Ref. [34]

is a lot more diverse than that the classical sintering theory could capture. For example, a classical sintering model, such as Coble's sintering law, has to be based on an assumed sintering mechanism. It is widely believed that a dominating sintering mechanism exists which depends on the powder material, the particle size and the sintering temperature. For nano-particles however, different contact necks in a same powder compact could form different inter-particle boundaries and therefore sinter by different mechanisms. Specific surface energy is an important parameter because it is the total surface energy that drives sintering. For nano-powder however the specific surface energy of the powder material should include a term considering the atomic structure (roughness) of the particle surface, as it plays a major role. An encouraging result is that the classical framework of solid state physics appears being valid for nano-particles if one can capture the diversity, i.e. if one knows that a contact sinters by grain-boundary diffusion, then Coble's theory applies. The issue is how to predict which contact (or how many of them) sinters by which mechanism.

References

1. Pan, J.: Philos. Mag. Lett. **84**, 303–310 (2004)
2. Herring, C.: The Physics of powder metallurgy. Kingston, W.E. (eds.) McGraw-Hill Book Company Inc., New York (1951)
3. Bouvard D., McMeeking, R.: J. Am. Ceram. Soc. 79, 666–672 (1996)
4. Suo, Z.: Adv. Appl. Mech. **33**, 193–294 (1997)
5. Pan, J., Cocks, A.C.F., Kucherenko, S.: Proc. R. Soc. Lond. A **453**, 2161–2184 (1997)
6. Cocks, A., Gill, S., Pan, J.: Adv. Appl. Mech. **36**, 81–162 (1999)
7. Coble, R.L.: J. Appl. Phys. **41**, 4798–4807 (1970)
8. Pan, J., Cocks, A.C.F.: Acta Mater. **42**, 1223–1230 (1994)
9. Pan, J., Cocks, A.C.F.: Acta Metall. Mater. **43**, 1395–1406 (1995)
10. Mcmeeking, R., Kuhn, L.: Acta Metall. Mater. **40**, 961–969 (1992)
11. Du, Z., Cocks, A.C.F.: Acta Metall. Mater. **40**, 1969–1979 (1992)
12. Cocks, A.C.F., Pan, J.: Mech. Mater. **18**, 269–287 (1994)
13. Cocks, A.C.F.: Mech. Mater. **13**, 165–174 (1992)
14. Bernard-Granger, G., Addad, A., Fantozzi, G., Bonnefont, G., Guizard, C., Vernat, D.: Acta Mater. **58**, 3390–3399 (2010)
15. Ding, L., Davidchack, R.L., Pan, J.: Comput. Mater. Sci. **45**, 247–256 (2009)
16. Rankin, J., Sheldon, B.W.: Mater. Sci. Eng. A **A204**, 48–53 (1995)
17. Pan, J., Le, H., Kucherenko, S., Yeomans, J.A.: Acta Metall. **46**, 4671–4690 (1998)
18. Parhami, F., McMeeking, R.M., Cocks, A.C.F., Suo, Z.: Mech. Mater. **31**, 43–61 (1999)
19. Saitou, M.: Philos. Mag. Lett. **79**, 257–263 (1999)
20. Ch'ng, H.N., Pan, J.: Acta Mater. **55**, 813–824 (2007)
21. Suryanarayana, C.: Inter. Mater. Rev. **40**, 41–64 (1995)
22. Mayo, M.J.: Inter. Mater. Rev. **41**, 85–115 (1996)
23. Johnson, K.L., Kendall, K., Roberts, A.D.: Surface energy and the contact of elastic solids. Proc. R. Soc. Lond. Ser. A Math. Phys. Sci. **324**, 301–313 (1971)
24. Derjaguin, B.V., Muller, V.M., Toporov, Y.P.: J. Colloid Interface Sci. **53**, 314–326 (1975)
25. Tabor, D.: J. Colloid Interface Sci. **58**, 2–13 (1977)
26. Maugis, D.J.: J. Colloid Interface Sci. **150**, 243–269 (1992)
27. Li, F., Pan, J., Sinka, C.: J. Mech. Phys. Solids **57**, 81194–81208 (2009)
28. Li, F., Pan, J., Sinka, C.: Mech. Mater. **43**, 157–167 (2011)
29. Slamovich, E.B., Lange, F.F.: J. Am. Ceram. Soc. **75**, 2498–2508 (1992)
30. Kingery, W.D., Francois, B.: The sintering of crystalline oxides. I. Interaction between grain boundaries and pores. In: Kuczynski, G.C., et al. (eds.) Sintering Related Phenomena, pp. 471–496. Gordon and Breach, New York (1967)
31. Kingery, W.D.: J. Appl. Phys. **30**, 301–306 (1959)
32. Flinn, B.D., Bordia, R.K., Zimmermann, A., Rodel, J.: J. Eur. Ceram. Soc. **20**, 2561–2568 (2000)
33. Pan, J., Ch'ng, H.N., Cocks, A.C.F.: Mech. Mater. **37**, 705–721 (2005)
34. Pan, J., Cocks, A.C.F., Rodel, J., Huang, R., and Ch'ng, H.N.: J. Am. Ceram. Soc. 92, 1414–1418 (2009)

http://www.springer.com/978-3-642-31008-9

Sintering
Mechanisms of Convention Nanodensification and Field Assisted Processes
Castro, R.; van Benthem, K. (Eds.)
2013, XII, 240 p., Hardcover
ISBN: 978-3-642-31008-9